BIOCHEMISTRY
including biophysical chemistry & molecular biology

Article

pubs.acs.org/biochemistry

Magnesium-Induced Nucleophile Activation in the Guanylyltransferase mRNA Capping Enzyme

Robert V. Swift,[†] Chau D. Ong,[‡] and Rommie E. Amaro*,[†]

[†]Department of Chemistry and Biochemistry, University of California, San Diego, La Jolla, California, 92093, United States
[‡]Lake Erie College of Osteopathic Medicine, 5000 Lakewood Ranch Boulevard, Brandenton, Florida 34211, United States

Supporting Information

ABSTRACT: The mRNA guanylyltransferase, or mRNA capping enzyme, cotranscriptionally caps the 5′-end of nascent mRNA with GMP during the second reaction in a set of three enzymatic reactions that result in the formation of an N7-methylguanosine cap during mRNA maturation. The mRNA capping enzyme is characterized, in part, by a conserved lysine nucleophile that attacks the α-phosphorus atom of GTP, forming a lysine−GMP intermediate. Experiments have firmly established that magnesium is required for efficient intermediate formation but have provided little insight into the requirement's molecular origins. Using empirical and thermodynamic integration pK_a estimates, along with conventional molecular dynamics simulations, we show that magnesium binding likely activates the lysine nucleophile by increasing its acidity and by biasing the deprotonated nucleophile into conformations conducive to intermediate formation. These results provide additional functional understanding of an important enzyme in the mRNA transcript life cycle and allow functional analogies to be drawn that affect our understanding of the metal dependence of related superfamily members.

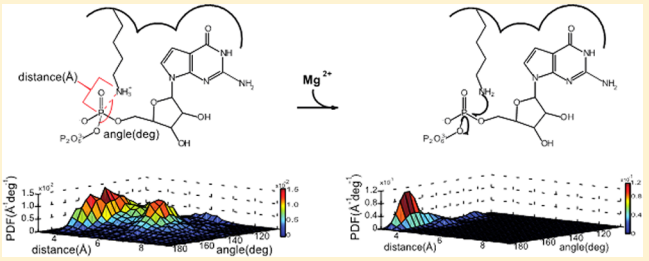

During transcription, within the nuclei of eukaryotic cells, GTP-dependent mRNA capping enzymes, members of the nucleotidyltransferase superfamily, participate in the addition of an N7-methyl-GMP cap to the 5′-end of nascent mRNA, a critical modification that plays several essential roles in the functional cycle of mRNA. Cap recognition is essential in mRNA splicing, transcript stability, nuclear export, and ribosomal translation initiation.[1−3] Because of its fundamental role in many of the events responsible for the normal flow of biologic information, the presence of an mRNA cap is essential in all eukaryotic cell types examined thus far.[4−9] Cap formation occurs by a set of three sequential enzymatic reactions; the mRNA capping enzyme conducts the second of these. During the first step, the 5′-phosphate is hydrolyzed from nascent mRNA by a triphosphatase. In the second step, the resulting 5′-diphosphate end is guanylated by a guanylyltransferase, or mRNA capping enzyme. Finally, during the third step, the N7 atom is methylated by a methyltransferase. GTP-dependent mRNA capping enzymes belong to a larger superfamily of enzymes called the nucleotidyltransferase superfamily, whose members also include ATP- and NAD^+-dependent DNA ligases and ATP-dependent RNA ligases.[10] Members share common structural features and catalyze reactions following similar mechanisms.[10]

Biochemical,[11,12] structural,[13] and kinetic[14] studies independently demonstrated that a magnesium ion is required for the capping enzyme to efficiently catalyze GMP transfer. Following GTP binding, the first chemical step of the reaction occurs when a conserved lysine nucleophile attacks the α-phosphorus atom of GTP, displacing pyrophosphate and forming a lysine−GMP intermediate (Figure 1). Following the release of pyrophosphate, nascent mRNA binds to the intermediate, and GMP is transferred from the lysine nucleophile to the mRNA 5′-phosphate during the second and final chemical step of the reaction (Figure 1). Although magnesium binding is a known prerequisite of both chemical steps,[14] the molecular origins of the requirement are ambiguous, and several possible

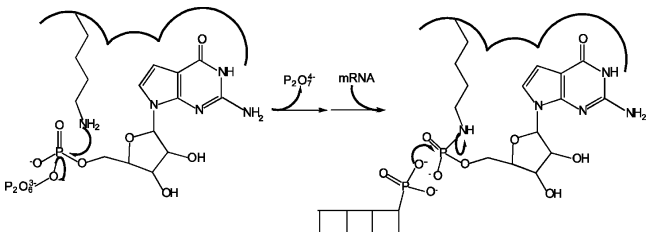

Figure 1. Guanylyltransferase mRNA capping mechanism. Following GTP binding, a conserved lysine nucleophile attacks the α-phosphorus atom of GTP, displacing pyrophosphate, resulting in the formation of a lysine−GMP intermediate. After the release of pyrophosphate and the subsequent binding of nascent mRNA, GMP is transferred from the lysine nucleophile to the mRNA 5′-phosphate completing the reaction.

Received: September 9, 2012
Revised: November 28, 2012
Published: December 4, 2012

explanations may suffice.[15] For example, assuming the first chemical step is an associative in-line attack,[16,17] the divalent magnesium cation may stabilize the negative charge present in the pentavalent transition state. Magnesium binding may also influence active-site geometry, optimally orienting the lysine nucleophile and pyrophosphate leaving group for formation of the lysine−GMP intermediate. Still another possibility is that magnesium binding increases the acidity of the lysine nucleophile, effectively increasing the concentration of the reactive enzyme. This is not an exhaustive list, and the possibilities given may all enhance catalysis to varying extents.

In this work, we explore the influence of magnesium binding on activating the lysine nucleophile during the first chemical step in the mRNA capping reaction. We examine how magnesium binding may affect lysine nucleophile acidity and influence the conformational distribution of the deprotonated lysine nucleophile. Specifically, empirical pK_a estimates and thermodynamic integration (TI) were used to estimate changes in lysine nucleophile acidity that may occur upon magnesium binding. Additionally, conventional molecular dynamics (MD) simulations were conducted in the presence and absence of magnesium to determine the influence of magnesium binding on the distance between the nucleophile and electrophile, as well as the angle formed by the nucleophile, electrophile, and leaving group. Throughout this work, structures from *Paramecium bursaria Chlorella* virus 1 (PBCV-1), the smallest functional mRNA capping enzyme known,[11,13] were used.

MATERIALS AND METHODS

Empirical pK_a Estimates. PROPKA3[18−21] was used to conduct empirical pK_a estimates. PROPKA3 benefits from explicitly incorporating the columbic interactions that arise from mutually titrating residues via the Tanford−Roxby scheme,[20,22] but it suffers from implicit estimations of the conformational reorganization that alter a titrating residue's microenvironment and affect its pK_a.[23] Consequently, titrations in which conformational reorganization plays a significant role may be inaccurately estimated. To conduct the PROPKA3 estimates, a model of the magnesium-bound GTP complex was first constructed from chain B of Protein Data Bank (PDB) entry 1ckm and chain B of PDB entry 1ckn.[13] Using the root-mean-square deviation trajectory tool in VMD,[24] the two chains were aligned by their α-carbon atoms. Following alignment, the magnesium was positioned in chain B of PDB entry 1ckm to overlap with the location of manganese from chain B of PDB entry 1ckn. This model, along with chain B of PDB entry 1ckm, was submitted to the PROPKA server, and the results were used to estimate the effects of magnesium binding on the acidity of the lysine nucleophile.

Thermodynamic Integration (TI). TI,[25,26] which relies on MD simulations,[26] more adequately captures the conformational reorganization that may occur upon titration of a residue. However, as MD simulations rely on classical mechanics to propagate system dynamics, traditionally, only a single residue of interest may change protonation state, while the protonation states of other residues remain fixed.[27−29] Hence, despite more accurately modeling conformational affects, TI suffers from the complete neglect of coupled titration. While neither PROPKA nor TI perfectly captures the physics of multisite titration and neither is likely to give a completely accurate answer, their trends should provide a qualitatively reasonable understanding of the effects of magnesium binding on the acidity of the lysine nucleophile. Below, we develop thermodynamic integration in greater detail.

The change in lysine nucleophile acidity upon magnesium binding is measured by the extent of proton dissociation in the presence and absence of bound magnesium, as described by the two reactions in Figure 2. The extent of proton dissociation in

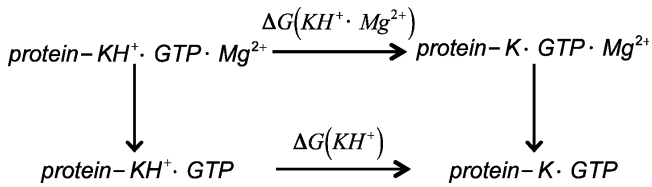

Figure 2. Thermodynamic cycle linking lysine nucleophile deprotonation in the presence and absence of magnesium bound in the active site.

each reaction is measured by the reaction equilibrium constant, K_a, which is related to the free energy change, ΔG:

$$\Delta G = -\frac{1}{\beta}\ln(K_a) \tag{1}$$

where $\beta^{-1} = RT$, with R being the universal gas constant and T the temperature. Using eq 1, the pK_a, defined as the negative log of the equilibrium constant, is expressed

$$\mathrm{p}K_a = \frac{\beta}{\log(e)}\Delta G \tag{2}$$

where the extent of nucleophile deprotonation upon magnesium binding, relative to the extent of deprotonation in the absence of magnesium, can be formulated in terms of the double free energy difference [$\Delta\Delta G = \Delta G(\mathrm{KH^+{\cdot}Mg^{2+}}) - \Delta G(\mathrm{KH^+})$], which is given by the thermodynamic cycle in Figure 2:

$$\Delta\mathrm{p}K_a = \frac{\beta}{\log(e)}\Delta\Delta G \tag{3}$$

where the pK_a difference, ΔpK_a, is given by $\mathrm{p}K_a(\mathrm{KH^+{\cdot}Mg^{2+}}) - \mathrm{p}K_a(\mathrm{KH^+})$.

Thermodynamic integration (TI) was used to estimate the double free energy difference in eq 3. In TI, the potential energy is expressed as a function of a coupling parameter, λ, which ranges from zero to one between end points. Assuming negligible volume changes along the transformation pathway, *NPT* and *NVT* results are equivalent, and the free energy change between pathway end points is expressed as

$$\Delta G = \int_{\lambda=0}^{\lambda=1} \left\langle \frac{\partial U}{\partial \lambda} \right\rangle_{\lambda} \mathrm{d}\lambda \tag{4}$$

Each free energy difference was calculated in three steps. First, the side chain of the positively charged, protonated lysine nucleophile was electrostatically decoupled from its environment by scaling the atomic partial charges to zero. Next, by scaling the van der Waals potential to zero, we annihilated the nonbonded interactions between one of the side chain amine protons and the surroundings. Last, the atomic partial charges of the deprotonated lysine side chain were scaled from zero to one, electrostatically coupling the side chain and surroundings. The integrand of eq 4 was estimated at 19 equally spaced λ values and numerically integrated using the trapezoidal rule for each transformation.

Integrand averages in eq 4 were estimated by MD simulations performed with the sander program in version 10 of the Amber simulation suite.[30] The GTP-bound system was constructed from chain B of PDB entry 1ckm. The magnesium-bound GTP complex was built using the model described in the Empirical pKa Estimates. With the exception of the lysine nucleophile, K82, which was protonated in both systems, protonation states were predicted using the PROPKA server. The Amber 99 force field,[31] with the Stony Brook corrections,[32] was used to describe the protein, while the Meagher−Carlson parameters were used to describe GTP.[33] Magnesium was represented by the Oelschlaeger−Warshel parameters, which delocalize charge over a central atom and six cationic dummy atoms, providing a more accurate depiction of divalent metal ion electrostatics and geometry.[34] While the presence of divalent magnesium may result in some charge redistribution for surrounding residues, we assumed the effects would be modest and neglected them. Ultimately, the validity of this assumption is subjective. However, as our results, discussed below, provide a reasonable interpretation of macroscopic observables consistent with generally accepted principles of enzyme mechanism, neglecting charge redistribution effects is a sensible, simplifying assumption for this study. Each system was immersed in a pre-equilibrated box of TIP3P water[35] that provided a 10 Å buffer between the longest protein dimension and the water box edge along the *x*-, *y*-, and *z*-axes. The systems were brought to electric neutrality by the addition of sodium ions. At each λ value, systems were minimized for 1000 steps using the steepest descent algorithm. To equilibrate system density, simulation for 100 ps at 1 atm and 300 K was conducted. Averaging followed and was performed over 2.25 ns of simulation in the *NVT* ensemble at 300 K; data points were sampled every 50 ps. A 1 fs time step was used in both ensembles. The temperature was controlled using a Langevin thermostat[36] with a collision frequency of 5 ps^{-1}, and the pressure was controlled with a Berendsen barostat.[37] An 8 Å nonbonded cutoff was used, and long-range electrostatics were evaluated by the PME method[38] with default grid spacing. Charge coupling contributions due to self-interactions between periodic images are essentially identical along the legs of the thermodynamic cycle and can be neglected.[39] To prevent the so-called end point catastrophe,[40] a soft-core potential[41] was used to perform simulations that scaled the van der Waals potential. All standard errors were calculated using distributions generated by bootstrap resampling the data, with replacement.[42]

Conventional MD Simulations. To probe the effects of magnesium binding on active-site geometry, additional GTP-bound simulations were constructed both with and without bound magnesium. In all simulations, the lysine nucleophile was modeled in a deprotonated, neutrally charged state. Each model was immersed in an explicit water box; counterions were added, and force field parameters were assigned as described in the Thermodynamic Integration (TI) section. Simulations were conducted identically for both models. Following 1000 steps of steepest descent energy minimization, equilibration was conducted for 1 ns at 1 atm and 300 K before *NVT* simulation was conducted for 50 ns at 300 K. Temperature, pressure, nonbonded cutoffs, and long-range electrostatics were treated as described in the TI section. In both ensembles, a 2 fs time step was used; bond lengths between hydrogen and heavy atoms were constrained using the SHAKE algorithm.[43]

RESULTS

Magnesium-Induced pK_a Shift. The acidity change of the lysine nucleophile, K82, was estimated by calculating the pK_a shift upon magnesium binding using PROPKA and TI. PROPKA is a rapid empirical approach that utilizes a single structure but accounts for cotitrating residues, while TI approximates ensemble averages using MD simulations but neglects cotitration. Though neither is expected to be completely accurate, the trends provide qualitative insight into the effects of magnesium binding on lysine nucleophile acidity. PROPKA estimates were evaluated using a GTP-bound crystal of the PBCV-1 mRNA capping enzyme, with and without a bound magnesium ion, whose position was modeled. The position was chosen to overlap with a manganese ion, which was observed in an enzyme−GMP intermediate formed by soaking the GTP-bound crystal in a solution of manganese chloride; the choice is reasonable because of the high degree of structural conservation between the lysine−GMP intermediate and the GTP-bound crystal structures.[13] Similarly, TI−MD simulations were conducted on the GTP-bound structures, with and without the modeled magnesium ion.

PROPKA predicts that magnesium binding facilitates K82 deprotonation. In the absence of bound magnesium, the predicted K82 pK_a is 14.51. Upon introduction of magnesium into the GTP-bound crystal structure, the predicted pK_a value decreases by 6.6 units to 7.89, indicating the predicted fraction of K82 in the deprotonated state increases by >6 orders of magnitude (Table 1).

Table 1. Comparing pK_a Prediction Methods[a]

method	pK_a without Mg^{2+}	pK_a with Mg^{2+}	ΔpK_a
PROPKA	14.51	7.89	−6.6
TI	–	–	−4.2 ± 0.3

[a]For the PROPKA results, ΔpK_a was determined by subtracting the value without Mg^{2+} from the value with Mg^{2+}. PROPKA is deterministic and yields a single value for a single structure, so no statistical error is reported. For the TI results, ΔpK_a was determined using eq 3 and the error calculated with standard propagation techniques.

Similarly, TI predicts that magnesium binding facilitates K82 deprotonation. The time series of the double free energy change, $\Delta\Delta G$, which was determined by subtracting the free energy change of deprotonating K82 in the GTP-bound state from the free energy change of deprotonating K82 in the GTP-magnesium-bound state, is reported in Figure 3. The double free energy change reaches a plateau after roughly 1 ns, taking a final value of −5.7 ± 0.5 kcal/mol after 2.25 ns. The negative double free energy change predicts that it is thermodynamically more favorable for K82 to release a proton following magnesium binding. Consistent with these predictions, the pK_a of K82 is expected to decrease by 4.2 ± 0.3 units after magnesium binds (Table 1). The increased acidity would cause the deprotonated fraction of K82 to increase by >4 orders of magnitude, a result consistent with the PROPKA estimates.

Magnesium Influences Active-Site Geometry. The putative effects of magnesium binding on the relative position and orientation of the lysine nucleophile and pyrophosphate leaving group were assessed by two 50 ns MD simulations of the GTP-bound and GTP-magnesium-bound states. The magnesium position was modeled as described in Magnesium-Induced pKa Shift. In both simulations, K82 was

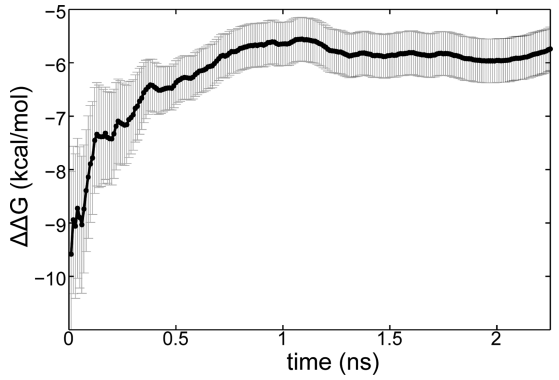

Figure 3. Double free energy change ($\Delta\Delta G$) time series. $\Delta\Delta G$ was determined by subtracting the change in free energy of deprotonating the lysine nucleophile GTP-bound state from the change in free energy of deprotonating the lysine nucleophile in the GTP-magnesium-bound state and is described in the legend of Figure 2. The standard error is reported.

represented in the deprotonated or neutral charge state, which is expected to mimic the state that reacts with the α-phosphorus atom of GTP. The relative position between the lysine nucleophile and α-phosphorus electrophile was determined by measuring the distance between the NZ atom of K82 and the PA atom of GTP (Figure 4B). Similarly, the relative orientation of the nucleophile and pyrophosphate leaving group was determined by measuring the angle formed among the NZ nucleophile atom of K82, the PA electrophile atom of GTP,

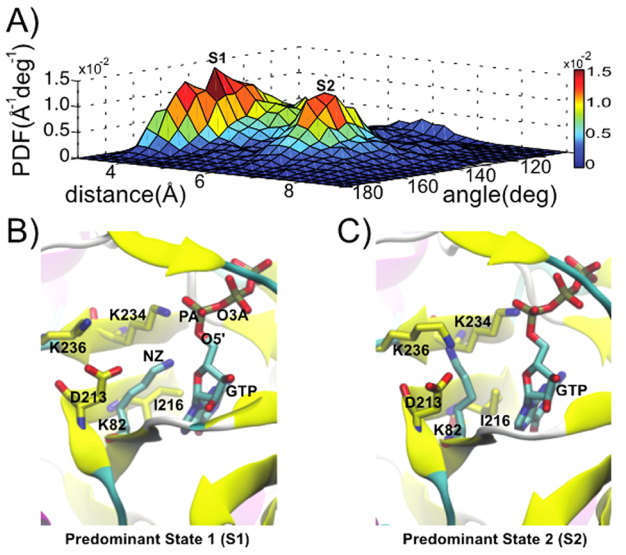

Figure 4. Non-magnesium-bound active-site geometry. (A) Two-dimensional probability distribution function (PDF) showing two predominant states, S1 and S2: distance marks the separation of the NZ nucleophile atom of K82 and the PA electrophile atom of GTP; angle indicates the angle formed by the NZ nucleophile, the PA electrophile, and the O3A atom, the first atom of the pyrophosphate leaving group. Each of these atoms is labeled in panel B. (B) Representative conformation from the predominant state with the smaller nucleophile−electrophile separation (S1). (C) Representative conformation from the predominant state with the larger nucleophile−electrophile separation (S2). In panels B and C, a pocket formed by K236, K234, D213, and I216 is shown with yellow carbon atoms while the carbon atoms of K82 and GTP are colored cyan.

and the O3A atom of GTP, the first atom of the pyrophosphate leaving group (Figure 4B).

Magnesium binding is predicted to shorten the distance between the nucleophile and electrophile and increase the angle formed by the nucleophile, electrophile, and leaving group. Two-dimensional probability distribution functions (PDFs) that report the probability of a given distance and angle occurring simultaneously are shown in Figures 4A and 5A for

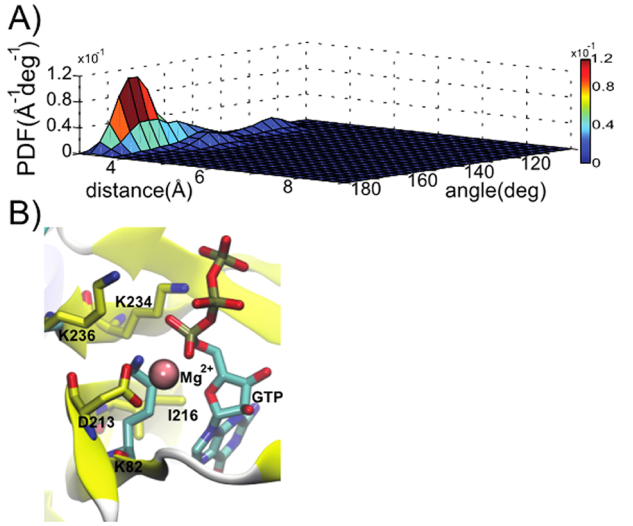

Figure 5. Magnesium-bound active-site geometry. (A) Two-dimensional probability distribution function (PDF) showing one predominant state: distance and angle are as defined in the legend of Figure 4A. (B) Representative conformation from the predominant state. Magnesium is shown as a magenta sphere. For reference, K236, K234, D213, and I216 are colored yellow. Carbon atoms of K82 and GTP are colored cyan.

the non-magnesium-bound and magnesium-bound simulations, respectively; the time series from which these results were derived, and the corresponding one-dimensional histogram distributions are shown in the Supporting Information.

Figure 4A shows that in the absence of magnesium, the lysine nucleophile predominantly samples two states, one with an average nucleophile−electrophile separation of 4.5 Å that takes on values as small as 3.2 Å (labeled S1 in Figure 4A) and the other with an average separation of 6.7 Å with values as large as 9.7 Å (labeled S2 in Figure 4A). In both states, the angle formed among the nucleophile, the electrophile, and the leaving group is approximately normally distributed, with an average value of 141° (Figure 4A). In the state with the smaller nucleophile−electrophile separation, S1, the K82 side chain nitrogen atom interacts with the O5′ atom of GTP (Figure 4B). The state with greater nucleophile−electrophile separation, S2, is formed when the K82 side chain moves away from GTP, likely because of electrostatic repulsion, into a pocket formed by the K234, K236, D213, and I216 side chains (Figure 4C). In contrast, Figure 5A shows that upon magnesium binding, the lysine nucleophile occupies predominantly one state characterized by an average nucleophile−electrophile separation of 3.5 Å that takes values as short as 2.9 Å and as long as 4.7 Å (Figure 5A). The angle formed between the nucleophile, electrophile, and leaving group is roughly normally distributed with an average value of 160°, though angles of up to 179.8° occur (Figure 5A). This state is stabilized by electrostatic

interactions between the negatively charged K82 side chain nitrogen atom and the divalent magnesium cation (Figure 5B).

DISCUSSION

Structural, biochemical, and kinetic reports firmly established that magnesium is required for the mRNA capping enzyme to efficiently catalyze lysine−GMP intermediate formation but have provided little insight into the requirement's molecular origins. The computational results presented here strongly implicate magnesium in lysine nucleophile activation, facilitating the formation of the lysine−GMP intermediate (Figure 1). Magnesium activation is predicted to occur with an increase in nucleophile acidity and by biasing the deprotonated nucleophile in conformations conducive to intermediate formation. These results provide additional functional understanding of an important enzyme in the mRNA transcript life cycle and allow functional analogies to be drawn that affect our understanding of the metal dependence of related superfamily members, points we discuss in greater detail below.

Magnesium binding activates the lysine nucleophile, in part, by increasing the fraction of the nucleophile in the deprotonated, reactive state. This result is readily understood in terms of electrostatic arguments and is consistent with both pK_a prediction methods employed. Prior to magnesium binding, a significant fraction of the lysine nucleophile is likely protonated, in an unreactive, metastable state. In this state, elucidated by X-ray crystallography,[13] the lysine lacks a reactive electron pair and is positively charged, creating favorable interactions with the nearby, negatively charged GTP triphosphate tail. Magnesium is predicted to bind within 4 Å of the lysine nucleophile, resulting in an electrostatically unfavorable interaction that can be mitigated by lysine deprotonation, consistent with the predicted downward shifts in pK_a (Table 1). Deprotonation exposes an electron pair and, assuming the deprotonated nucleophile achieves a reactive conformation, allows reaction with the α-phosphorus electrophile, leading to formation of the lysine−GMP intermediate. Thus, with an increase in the concentration of the deprotonated nucleophile, magnesium increases the concentration of the enzyme that is able to form the lysine−GMP intermediate.

Following deprotonation, magnesium increases the chances that the nucleophile will achieve a reactive conformation, further facilitating lysine−GMP intermediate formation. Phosphoryl transfer reactions are known to follow three distinct pathways: dissociative, concerted, or addition−elimination.[16] In all three pathways, the approaching nucleophile is oriented in-line with the leaving group, and the angle formed by the nucleophile, electrophile, and leaving group is 180°. When lysine deprotonation occurs in the absence of magnesium, the simulation results presented here indicate that the deprotonated nucleophile will seldom be both proximal to the electrophile and in-line with the leaving group. For example, in the absence of magnesium, the nucleophile frequently moved to an unreactive distance, away from the electrophile, into an adjacent active-site pocket (Figure 4A,C). This rearrangement is likely due to the electrostatic repulsion between the nucleophile and the GTP α-phosphate oxygen atoms. On occasions when the deprotonated lysine nucleophile approached the electrophile, it shifted below the reactive, in-line position to a position near the GTP O5′ atom (Figure 4C), also likely because of electrostatic repulsion. Therefore, although proximal-in-line conformations conducive to intermediate formation existed, these conformations were rarely sampled. This is apparent in the diffuse distance−angle distribution, which is sparsely populated for distances of <3.5 Å and angles near 180° (Figure 5A). These reactive conformations are made more rare by the smaller fraction of deprotonated lysine−nucleophile intermediate expected in the absence of magnesium. Consequently, the chances of lysine intermediate formation occurring in the absence of magnesium are small, consistent with the available experimental data. In contrast, when lysine deprotonation occurs when magnesium is bound, the deprotonated nucleophile spends more time proximal to the electrophile and in-line with the leaving group, conformations conducive to lysine−GMP intermediate formation. For example, likely because attractive electrostatic interactions between the nucleophile and the divalent magnesium ion offset repulsion from the α-phosphate oxygen atoms, the lysine nucleophile stays highly localized, frequently sampling conformations near the electrophile (Figure 4A,B). The greater frequency is evident in the more concentrated distance−angle distribution, which is reasonably populated for distances of <3.5 Å and angles near 180° (Figure 4A). These reactive conformations are made more abundant by the greater fraction of deprotonated lysine−nucleophile intermediate expected in the presence of magnesium. Thus, magnesium binding enhances the chances of lysine intermediate formation. Indeed, it is only when a GTP-bound crystal is soaked in a solution of manganese chloride, providing manganese, a surrogate for magnesium that diffracts X-rays more strongly, that the lysine−GMP intermediate is formed.[13]

The computational results reported here strongly imply that magnesium binding activates the lysine nucleophile prior to intermediate formation; however, magnesium-induced catalytic enhancement may originate from additional sources, such as transition state stabilization. For example, during associative phosphoryl transfer,[16,17] in which the lysine−nucleophile intermediate approaches the electrophile prior to leaving group departure, the reacting phosphate passes through a planar, pentavalent state. This state exhibits a formal charge of −2 or −3, on the phosphate nonbridging oxygen atoms, depending on whether the reaction follows a concerted or addition−elimination pathway, respectively. In each case, the presence of a divalent magnesium cation may provide significant electrostatic stabilization as the pentavalent state forms, which would provide catalytic enhancement by lowering each pathway's activation barrier. In a dissociative process, on the other hand, the pyrophosphate group departs prior to the lysine nucleophile reacting with the α-phosphorus electrophile. This results in the departing leaving group accumulating negative charge, which the divalent magnesium cation may also be positioned to stabilize. Therefore, while the exact phosphoryl transfer mechanism is unclear, it is physically reasonable to expect the magnesium ion to participate in some form of transition state stabilization.

While the results reported in this work are specific to the PBCV-1 mRNA capping enzyme, sequence and structural homology to mRNA capping enzymes from other species,[44−46] and to other nucleotidyltransferase superfamily members, allows functional analogies to be drawn that affect our understanding of metal dependence in these enzymes as well. For instance, significant homology among mRNA capping enzymes makes it likely that the magnesium-induced lysine activation described in this work is broadly applicable to all mRNA capping enzymes. This is supported, at least in part, by previously reported mutational analysis. D213, which is

predicted to coordinate magnesium (Figure 4B), is conserved among mRNA capping enzymes from *Schizosaccharomyces pombe*, *Saccharomyces cerevisiae*, *Candida albicans*, *Mus musculus*, and *Homo sapiens*[44] and was found to be essential during mutational studies of *M. musculus*[44] and *S. cerevisiae*[45] capping enzymes. It is likely that mutating this residue destabilizes magnesium binding, significantly reducing or completely eliminating magnesium uptake and preventing lysine−GMP intermediate formation. Similarly, structural homology with related nucleotidyltransferase superfamily members implies that magnesium may activate the lysine nucleophile in a manner analogous to that found for the PBCV-1 mRNA capping enzyme. For example, when ATP-dependent RNA ligase 1 from T4 bacteriophage was crystallized with an unreactive AMPCPP analogue, two divalent metals were found in the active site.[47] A calcium ion was found adjacent to the α-phosphate in a position analogous to that of the modeled magnesium in this work, while a magnesium ion was coordinated between the β- and γ-phosphates (Figure 6).

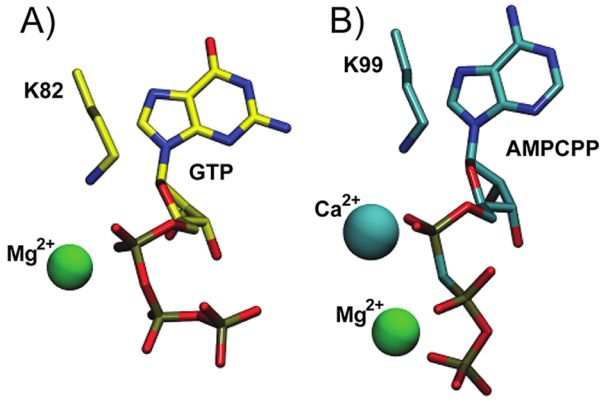

Figure 6. Metal position homology among nucleotidyltransferase superfamily members. (A) PBCV-1 mRNA capping enzyme showing the position of the modeled magnesium ion, the lysine nucleophile, and GTP. Carbon atoms are colored yellow. (B) T4 phage RNA ligase showing the position of cocrystallized calcium and magnesium ions, the lysine nucleophile, and an unreactive ATP analogue, AMPCPP. Carbon atoms are colored cyan.

The positions of the lysine nucleophiles are very similar in the two structures, and because the two enzymes each form a lysine−nucleoside−monophosphate intermediate and have significantly conserved active-site residues, it is plausible that a divalent metal bound at the calcium site activates the lysine nucleophile in a manner identical to that described in this work. Moreover, metal ions have been found, or metal-binding sites proposed, adjacent to the α-phosphate in other superfamily member active sites.[48−50] While these structures correspond to later mechanistic steps, metal reconfiguration is thought to occur following intermediate formation, implying a nucleoside triphosphate metal configuration similar to those shown in Figure 6; consequently, it is likely that the metal ion-induced lysine activation described in this work holds across all enzyme types within the superfamily.

CONCLUSIONS

Using empirical and thermodynamic integration pK_a estimates, along with conventional MD simulations, we showed how magnesium binding may activate the lysine nucleophile through formation of the lysine−GMP intermediate during the first chemical step of the PBCV-1 mRNA capping enzyme reaction. Consistent with simple electrostatic arguments, both pK_a estimation methods predict that magnesium binding increases lysine nucleophile acidity, enlarging the fraction of the nucleophile in the deprotonated, reactive state. Conventional MD simulations predict that magnesium biases the deprotonated nucleophile to more heavily favor conformations conducive to intermediate formation. While these results improve our functional understanding of the *Chlorella* virus capping enzyme, the smallest known functional capping enzyme, homology between capping enzymes across species implies that the results are applicable to all capping enzymes. Similarly, structural and mechanistic homology among members of the nucleotidyltransferase superfamily makes it likely that the magnesium activates the lysine nucleophile of these enzymes as well. While these broader conclusions need to be independently validated on an enzyme-by-enzyme basis, this work provides a platform to understand the magnesium requirements in the PBCV-1 mRNA capping enzyme and possibly other superfamily enzymes.

ASSOCIATED CONTENT

Supporting Information

Plots of the distance and angle time series used to construct Figures 4A and 5A and corresponding one-dimensional histograms. This material is available free of charge via the Internet at http://pubs.acs.org.

AUTHOR INFORMATION

Corresponding Author

*Telephone: (858) 534-9629. Fax: (858) 534-9645. E-mail: ramaro@ucsd.edu.

Funding

This work was supported by the National Institutes of Health Director's New Innovator Award Program DP2-OD007237.

Notes

The authors declare no competing financial interest.

ACKNOWLEDGMENTS

R.V.S. thanks members of the Amaro group for useful discussion during manuscript development.

REFERENCES

(1) Izaurralde, E., Lewis, J., McGuigan, C., Jankowska, M., Darzynkiewicz, E., and Mattaj, I. W. (1994) A nuclear cap binding protein complex involved in pre-mRNA splicing. *Cell 78*, 657−668.

(2) Hamm, J., and Mattaj, I. W. (1990) Monomethylated cap structures facilitate RNA export from the nucleus. *Cell 63*, 109−118.

(3) Shatkin, A. J. (1985) mRNA cap binding proteins: Essential factors for initiating translation. *Cell 40*, 223−224.

(4) Mao, X., Schwer, B., and Shuman, S. (1995) Yeast mRNA cap methyltransferase is a 50-kilodalton protein encoded by an essential gene. *Mol. Cell. Biol. 15*, 4167−4174.

(5) Yue, Z., Maldonado, E., Pillutla, R., Cho, H., Reinberg, D., and Shatkin, A. J. (1997) Mammalian capping enzyme complements mutant *Saccharomyces cerevisiae* lacking mRNA guanylyltransferase and selectively binds the elongating form of RNA polymerase II. *Proc. Natl. Acad. Sci. U.S.A. 94*, 12898−12903.

(6) Tsukamoto, T., Shibagaki, Y., Imajoh-Ohmi, S., Murakoshi, T., Suzuki, M., Nakamura, A., Gotoh, H., and Mizumoto, K. (1997) Isolation and characterization of the yeast mRNA capping enzyme β subunit gene encoding RNA 5′-triphosphatase, which is essential for cell viability. *Biochem. Biophys. Res. Commun. 239*, 116−122.

(7) Srinivasan, P., Piano, F., and Shatkin, A. J. (2003) mRNA capping enzyme requirement for *Caenorhabditis elegans* viability. *J. Biol. Chem. 278*, 14168−14173.
(8) Shafer, B., Chu, C., and Shatkin, A. J. (2005) Human mRNA cap methyltransferase: Alternative nuclear localization signal motifs ensure nuclear localization required for viability. *Mol. Cell. Biol. 25*, 2644−2649.
(9) Chu, C., and Shatkin, A. J. (2008) Apoptosis and autophagy induction in mammalian cells by small interfering RNA knockdown of mRNA capping enzymes. *Mol. Cell. Biol. 28*, 5829−5836.
(10) Shuman, S., and Lima, C. D. (2004) The polynucleotide ligase and RNA capping enzyme superfamily of covalent nucleotidyltransferases. *Curr. Opin. Struct. Biol. 14*, 757−764.
(11) Ho, C. K., Van Etten, J. L., and Shuman, S. (1996) Expression and characterization of an RNA capping enzyme encoded by *Chlorella* virus PBCV-1. *J. Virol. 70*, 6658−6664.
(12) Venkatesan, S., and Moss, B. (1982) Eukaryotic mRNA capping enzyme-guanylate covalent intermediate. *Proc. Natl. Acad. Sci. U.S.A. 79*, 340−344.
(13) Hakansson, K., Doherty, A. J., Shuman, S., and Wigley, D. B. (1997) X-ray crystallography reveals a large conformational change during guanyl transfer by mRNA capping enzymes. *Cell 89*, 545−553.
(14) Souliere, M. F., Perreault, J. P., and Bisaillon, M. (2008) Kinetic and thermodynamic characterization of the RNA guanylyltransferase reaction. *Biochemistry 47*, 3863−3874.
(15) Andreini, C., Bertini, I., Cavallaro, G., Holliday, G. L., and Thornton, J. M. (2008) Metal ions in biological catalysis: From enzyme databases to general principles. *J. Biol. Inorg. Chem. 13*, 1205−1218.
(16) Allen, K. N., and Dunaway-Mariano, D. (2004) Phosphoryl group transfer: Evolution of a catalytic scaffold. *Trends Biochem. Sci. 29*, 495−503.
(17) Fersht, A. (1999) *Structure and mechanism in protein science: A guide to enzyme catalysis and protein folding*, W. H. Freeman, New York.
(18) Li, H., Robertson, A. D., and Jensen, J. H. (2005) Very fast empirical prediction and rationalization of protein pK_a values. *Proteins 61*, 704−721.
(19) Bas, D. C., Rogers, D. M., and Jensen, J. H. (2008) Very fast prediction and rationalization of pK_a values for protein-ligand complexes. *Proteins 73*, 765−783.
(20) Olsson, M. H. M., Sondergaard, C. R., Rostkowski, M., and Jensen, J. H. (2011) PROPKA3: Consistent Treatment of Internal and Surface Residues in Empirical pK_a Predictions. *J. Chem. Theory Comput. 7*, 525−537.
(21) Sondergaard, C. R., Olsson, M. H. M., Rostkowski, M., and Jensen, J. H. (2011) Improved Treatment of Ligands and Coupling Effects in Empirical Calculation and Rationalization of pK_a Values. *J. Chem. Theory Comput. 7*, 2284−2295.
(22) Tanford, C., and Roxby, R. (1972) Interpretation of protein titration curves. Application to lysozyme. *Biochemistry 11*, 2192−2198.
(23) Fersht, A. R. (1972) Conformational equilibria in α- and δ-chymotrypsin. The energetics and importance of the salt bridge. *J. Mol. Biol. 64*, 497−509.
(24) Humphrey, W., Dalke, A., and Schulten, K. (1996) VMD: Visual molecular dynamics. *J. Mol. Graphics Modell. 14*, 33−38.
(25) Kirkwood, J. G. (1935) Statistical Mechanics of Fluid Mixtures. *J. Chem. Phys. 3*, 300−313.
(26) Frenkel, D., and Smit, B. (2007) *Understanding Molecular Simulation: From Algorithms to Applications*, Academic Press, New York.
(27) Simonson, T., Carlsson, J., and Case, D. A. (2004) Proton binding to proteins: pK_a calculations with explicit and implicit solvent models. *J. Am. Chem. Soc. 126*, 4167−4180.
(28) Xin, Y., and Hamelberg, D. (2010) Deciphering the role of glucosamine-6-phosphate in the riboswitch action of glmS ribozyme. *RNA 16*, 2455−2463.
(29) Warshel, A., Sussman, F., and King, G. (1986) Free energy of charges in solvated proteins: Microscopic calculations using a reversible charging process. *Biochemistry 25*, 8368−8372.
(30) Case, D. A., Trucks, A. D., Cheatham, T. E., III, Simmerling, C. L., Wang, J., Duke, R. E., Luo, R., Walker, R. C., Zhang, W., Merz, K. M., Roberts, B., Hayik, S., Roitberg, A., Seabra, G., Swails, J., Goetz, A. W., Kolossvai, I., Wong, K. F., Paesani, F., Vanicek, J., Wolf, R. M., Liu, J., Wu, X., Brozell, S. R., Steinbrecher, T., Gohlke, H., Cai, Q., Ye, X., Wang, J., Hsieh, M.-J., Cui, G., Roe, D. R., Mathews, D. H., Seetin, M. G., Salomon-Ferrer, R., Sagui, C., Babin, V., Luchko, T., Gusarov, S., Kovalenko, A., and Kollman, P. A. (2012) *Amber*, version 12, University of California, San Francisco.
(31) Wang, J., Cieplak, P., and Kollman, P. A. (2000) How Well Does a Restrained Electrostatic Potential (RESP) Model Perform in Calculating Conformational Energies of Organic and Biological Molecules? *J. Comput. Chem. 21*, 1049−1074.
(32) Hornak, V., Abel, R., Okur, A., Strockbine, B., Roitberg, A., and Simmerling, C. (2006) Comparison of multiple Amber force fields and development of improved protein backbone parameters. *Proteins 65*, 712−725.
(33) Meagher, K. L., Redman, L. T., and Carlson, H. A. (2003) Development of polyphosphate parameters for use with the AMBER force field. *J. Comput. Chem. 24*, 1016−1025.
(34) Oelschlaeger, P., Klahn, M., Beard, W. A., Wilson, S. H., and Warshel, A. (2007) Magnesium-cationic dummy atom molecules enhance representation of DNA polymerase β in molecular dynamics simulations: Improved accuracy in studies of structural features and mutational effects. *J. Mol. Biol. 366*, 687−701.
(35) Jorgensen, W. L., Chandrasekhar, J., Madura, J. D., Impey, R. W., and Klein, M. L. (1983) Comparison of Simple Potential Functions for Simulating Liquid Water. *J. Chem. Phys. 79*, 926−935.
(36) Loncharich, R. J., Brooks, B. R., and Pastor, R. W. (1992) Langevin dynamics of peptides: The frictional dependence of isomerization rates of N-acetylalanyl-N′-methylamide. *Biopolymers 32*, 523−535.
(37) Berendsen, H. J. C., Postma, J. P. M., Vangunsteren, W. F., Dinola, A., and Haak, J. R. (1984) Molecular-Dynamics with Coupling to an External Bath. *J. Chem. Phys. 81*, 3684−3690.
(38) Essmann, U., Perera, L., Berkowitz, M. L., Darden, T., Lee, H., and Pedersen, L. G. (1995) A Smooth Particle Mesh Ewald Method. *J. Chem. Phys. 103*, 8577−8593.
(39) Morgan, B. R., and Massi, F. (2010) Accurate Estimates of Free Energy Changes in Charge Mutations. *J. Chem. Theory Comput. 6*, 1884−1893.
(40) Beutler, T. C., Mark, A. E., Vanschaik, R. C., Gerber, P. R., and Vangunsteren, W. F. (1994) Avoiding Singularities and Numerical Instabilities in Free-Energy Calculations Based on Molecular Simulations. *Chem. Phys. Lett. 222*, 529−539.
(41) Steinbrecher, T., Mobley, D. L., and Case, D. A. (2007) Nonlinear scaling schemes for Lennard-Jones interactions in free energy calculations. *J. Chem. Phys. 127*, 214108.
(42) Mooney, C. Z., and Duval, R. D. (1993) *Bootstrapping: A Nonparameteric Approach to Statistical Inference*, Sage, Newbury Park, CA.
(43) Ryckaert, J. P., Ciccotti, G., and Berendsen, H. J. C. (1977) Numerical-Integration of Cartesian Equations of Motion of a System with Constraints: Molecular-Dynamics of N-Alkanes. *J. Comput. Phys. 23*, 327−341.
(44) Sawaya, R., and Shuman, S. (2003) Mutational analysis of the guanylyltransferase component of mammalian mRNA capping enzyme. *Biochemistry 42*, 8240−8249.
(45) Wang, S. P., Deng, L., Ho, C. K., and Shuman, S. (1997) Phylogeny of mRNA capping enzymes. *Proc. Natl. Acad. Sci. U.S.A. 94*, 9573−9578.
(46) Chu, C., Das, K., Tyminski, J. R., Bauman, J. D., Guan, R., Qiu, W., Montelione, G. T., Arnold, E., and Shatkin, A. J. (2011) Structure of the guanylyltransferase domain of human mRNA capping enzyme. *Proc. Natl. Acad. Sci. U.S.A. 108*, 10104−10108.
(47) El Omari, K., Ren, J., Bird, L. E., Bona, M. K., Klarmann, G., LeGrice, S. F., and Stammers, D. K. (2006) Molecular architecture and ligand recognition determinants for T4 RNA ligase. *J. Biol. Chem. 281*, 1573−1579.

(48) Nandakumar, J., Shuman, S., and Lima, C. D. (2006) RNA ligase structures reveal the basis for RNA specificity and conformational changes that drive ligation forward. *Cell 127*, 71−84.
(49) Odell, M., Sriskanda, V., Shuman, S., and Nikolov, D. B. (2000) Crystal structure of eukaryotic DNA ligase-adenylate illuminates the mechanism of nick sensing and strand joining. *Mol. Cell 6*, 1183−1193.
(50) Akey, D., Martins, A., Aniukwu, J., Glickman, M. S., Shuman, S., and Berger, J. M. (2006) Crystal structure and nonhomologous end-joining function of the ligase component of *Mycobacterium* DNA ligase D. *J. Biol. Chem. 281*, 13412−13423.